Research Article | Vol. 13, No. 2 / 1 Feb 2022 / Biomedical Optics Express 539
Biomedical Optics EXPRESS

Biosensing with a scanning planar Yagi-Uda antenna

NAVID SOLTANI,[1,2,*] ELHAM RABBANY ESFAHANY,[1,2] SERGEY I. DRUZHININ,[2,3] GREGOR SCHULTE,[2,3] JULIAN MÜLLER,[2,4] BENJAMIN BUTZ,[2,4] HOLGER SCHÖNHERR,[2,3] MARIO AGIO,[1,2,5] AND NEMANJA MARKEŠEVIĆ[1,6]

[1]*Laboratory of Nano-Optics, University of Siegen, Siegen 57072, Germany*
[2]*Research Center of Micro- and Nanochemistry and (Bio)Technology (Cμ), Siegen 57076, Germany*
[3]*Physical Chemistry I, University of Siegen, Siegen 57076, Germany*
[4]*Micro- and Nanoanalytics Group, University of Siegen, Siegen 57076, Germany*
[5]*National Institute of Optics (INO), National Research Council (CNR), Florence 50125, Italy*
[6]*Currently with Nanoscience Center, University of Jyväskylä, Jyväskylä 40014, Finland*
[*]*navid.soltani@uni-siegen.de*

Abstract: We investigate a model bioassay in a liquid environment using a *z*-scanning planar Yagi-Uda antenna, focusing on the fluorescence collection enhancement of ATTO-647N dye conjugated to DNA (deoxyribonucleic acid) molecules. The antenna changes the excitation and the decay rates and, more importantly, the emission pattern of ATTO-647N, resulting in a narrow emission angle (41°) and improved collection efficiency. We efficiently detect immobilized fluorescently-labeled DNA molecules, originating from solutions with DNA concentrations down to 1 nM. In practice, this corresponds to an ensemble of fewer than 10 ATTO-647N labeled DNA molecules in the focal area. Even though we use only one type of biomolecule and one immobilization technique to establish the procedure, our method is versatile and applicable to any immobilized, dye-labeled biomolecule in a transparent solid, air, or liquid environment.

1. Introduction

The detection of biomolecules at low concentrations [1,2] is crucial for the early-stage diagnostics of diseases. However, their interrogation is a real challenge since they are small and typically mixed with other types of molecules. They are detectable upon interaction with light or via other schemes; thus, various labeling and label-free techniques have been developed over the years [3–6].

To enhance the collection efficiency and improve the signal-to-noise ratio (SNR), different phenomena and techniques such as surface plasmon resonance [7], localized surface plasmon resonance [8,9], surface-enhanced Raman spectroscopy [10,11], optofluidic Fabry-Pérot cavities [12], nanogap antennas [13,14], and zero mode waveguides [15] have been employed.

In some cases, it is essential to label the biomolecule with fluorescence dyes. However, these suffer from blinking and photobleaching [16]. Moreover, they emit light like dipolar sources. This further means that a significant fraction of the emitted photons cannot be efficiently collected by optical elements. A practical approach to overcome this issue relies on optical antennas that can change the radiation pattern, enhance the excitation efficiency and the fluorescence quantum yield to improve the emission signal [17–20].

Most optical antennas demand precise positioning of the emitters and complicated fabrication and experimental procedures to observe a significant change in the radiation pattern. A planar optical Yagi-Uda antenna, which enhances the collection efficiency by beaming the fluorescent light into a narrow cone, has been recently proposed [21]. This system is easy to fabricate and it does not suffer from a demanding positioning with nanometer-scale precision. Namely, it is

#445402 https://doi.org/10.1364/BOE.445402
Journal © 2022 Received 11 Oct 2021; revised 8 Dec 2021; accepted 8 Dec 2021; published 3 Jan 2022

Biomedical Optics EXPRESS

only essential to immobilize emitters on a transparent substrate supported by a thin metal layer; otherwise, the translation in the (xy) plane does not play a crucial role. We further extended this idea to a z-scanning planar Yagi-Uda antenna, where we can control the vertical distance between the antenna elements to examine the optical properties of fluorescent beads [22].

In this work, we apply the scanning antenna approach for biosensing to detect short double-stranded DNA (dsDNA) molecules in a liquid, immobilized on a transparent surface. Although dsDNA molecules are not fluorescent, one of the strands in the pair features a single dye molecule, ATTO-647N (ATTO-TEC GmbH), which enables its detection. ATTO-647N is chosen because it is rather photo-stable and possesses a high fluorescence quantum yield. Despite the fact that we utilize ATTO-647N labeled dsDNA molecules as a toy model, we argue that this approach is general and that it can be applied to specific fluorescence-based bioassays.

2. Materials and methods

2.1. DNA strands and hybridization

Short dsDNA molecules are created in a hybridization process of the sequences purchased from Integrated DNA Technologies (DNA1: 5'-/5Biosg/ GCA CGA AAC CTG GAC ATG GGA ACA ATA -3' and DNA2: 5'-/5ATTO647NN/TAT TGT TCC CAT CTG GTC CAG GTT TCG TGC -3'). The sequences are modified and adjusted from Ref. [23]. In this process, 1 μL of 100 μM of DNA1 and 1 μL of 100 μM of DNA2 are mixed with 7 μL of pure water (MilliQ H_2O 18.2 MΩcm) and 1 μL of 1 mM NaCl in a micro-tube and left in a hot water bath (95 °C) to cool overnight. The described procedure ensures that the dsDNA constructs feature a single ATTO-647N fluorophore on one end and a biotin molecule on another.

2.2. Flow channels

A glass coverslip (PLANO, L42342 #1) is first rinsed with pure water and isopropanol and subsequently dried with compressed air. After the rinsing and drying steps, 15 minutes of UV-ozone cleaning (Bioforce UV/Ozone ProCleaner Plus) increase the hydrophilic character of the glass surface and promotes the attachment of proteins. A flow channel is eventually created on the glass coverslip, by placing two stripes of parafilm at a distance of approximately 5 mm and by gluing them to the surface by heating the glass coverslip on a hot plate above 60 °C. The flow channel prevents the solution to spread over the sample and it provides a controllable ATTO-647N labeled dsDNA immobilization process, which will be explained in the next step.

2.3. dsDNA attachment to the surface

The attachment of the ATTO-647N labeled dsDNA molecules in the flow channel consists of several steps [24,25], which we follow in the sample preparation process. Biotinylated bovine serum albumin (BSA) and neutravidin are purchased from Sigma-Aldrich (cat. no A-8549) and Thermo Scientific (31000), respectively, and dissolved in water to the concentration of 1 mg/mL, each. After pipetting 40 μL of BSA solution into the flow channel and the incubation time of 10 minutes, the surplus of material is washed by 400 μL (4 × 100 μL) of T50 (10 mM Tris and 50 mM NaCl). In the following steps, we add the same volumes of neutravidin and superblock (Thermo Scientic 37515), one after the other, with the same incubation time and washing procedures in between. The superblock prevents any non-specic binding.

Finally, 40 μL of a solution of ATTO-647N labeled dsDNA in T50 is added and left to incubate for 30 minutes leaving ample time for the attachment. The washing step at this point is particularly important to remove all free-floating fluorescent molecules, which could cause an unwanted background signal during the optical measurements. We prepare several different samples with different concentration of ATTO-647N labeled dsDNA in T50 ranging from 10 nM down to 10 pM.

Biomedical Optics EXPRESS

2.4. Fabrication of a planar Yagi-Uda antenna

A planar Yagi-Uda antenna consists of two main parts, a reflector, and a director [21]. We purchase glass substrates coated by 2 nm titanium and 10 nm gold (Platypustech, AU.0100.CSS Square Coverslips). The titanium layer is an adhesion layer, while the gold film plays the role of a director. The autofluorescence of gold film increases the background signal in the optical measurements, but it does not prevent an efficient detection of ATTO 647N (see Fig. S1).

The fluorescent molecules should be positioned at a distance in the range between $\lambda/6n$ and $\lambda/4n$ from the antenna elements in order to have the maximum beaming effect. Here, n represents the refractive index of the medium and λ is the emission wavelength in free space [21]. Therefore, an E-beam evaporation of a 75 nm thick SiO_2 layer over the gold film turns out as the most convenient method to form a transparent spacer, which in addition does not induce quenching.

The coverslip coated with 10 nm gold and 75 nm SiO_2 layers will be called the director substrate in the rest of the text. The standard procedure of the dsDNA attachment described for glass coverslips works well also for SiO_2 and in this case the flow channel is formed on the director substrate, following the procedure described earlier (director flow channel).

The reflector is created starting from a 250 μm gold wire (chemPUR, NO:009164), which is electrochemically etched (37% HCl) and then milled by Focused Ion Beam (FEI Helios Nanolab 600). This is the way to manufacture a flat mirror (10 μm diameter), which plays the role of a reflector.

The antenna elements are adjusted to be parallel to each other and the distance between the reflector and the substrate director can be varied by a piezo stage (Newport, NPM140SG). To fix the tilt angle and find a contact point, we observe the interference pattern caused by the phase shift between the reflected light from the director and the reflector using a CMOS camera (ZEISS AxioCam ERc 5s Rev.2) [22,26].

2.5. Optical setup and measurements

We detect ATTO-647N labeled dsDNA molecules with an epifluorescence microscope (Zeiss, Axio Observer 3) equipped with an oil-immersion objective (Zeiss, Plan-Apochromat 63x/1.4). To verify the success of the immobilization process, we use a wide-field imaging technique by adding a lens (WFL) before the objective into the excitation path. For the excitation, we utilize a pulsed diode laser at the wavelength of 636 nm (Picoquant, LDH-P-C-640B) with a repetition rate of 40 MHz. The collected light from the sample is sent through a set of filters; a long-pass (LP) (cutoff at 650 nm) and a band-pass (BP) (660-700 nm) filters to remove the reflected laser light and reduce the background.

A homemade module holding the gold wire is mounted on top of the microscope, which enables precise control over the distance between reflector and director using a piezo stage, as mentioned earlier. The center of the reflector is positioned directly above the focal spot of the laser, and it can move step-wise in the z-direction. A motorized stage (ASI, PZ-2000FT) controls the position of the director substrate (with ATTO-647N labeled dsDNA molecules immobilized on the surface) in the xy-directions.

At each piezo step, the emitted light is collected by the same objective and sent further either to single-photon avalanche diodes (SPADs) (Excelitas, SPCM-AQRH-TR) or to a CMOS camera (Andor, Zyla 4.2 Plus), depending on the type of experiment. For lifetime and intensity measurements, we direct light towards the SPADs, which are connected to a Time-Correlated Single-Photon Counting (TCSPC) device (PicoQuant, Pico Harp 300). To determine the radiation pattern of the molecules, light is sent to the CMOS camera with the back focal lens in front of it. It is also possible to replace the CMOS camera with a spectrometer (OceanOptics QE Pro) in order to check the emission spectrum of the molecule or the fluorescence background.

Biomedical Optics EXPRESS

3. Results

After the immobilization of ATTO-647N labeled dsDNA molecules on the glass coverslip flow channel, we use wide-field imaging to estimate the distribution and the number of attached molecules (Fig. 1(a)-(f)). The attachment process is random, therefore we can clearly observe the regions with the different densities of emitters. This becomes prominent once the DNA concentration in the incubated solution drops below 1 nM. The set of measurements is performed to understand the relation between the concentration of ATTO-647N labeled dsDNA molecules in solution and the number of molecules that are eventually attached to the substrate. To determine the fluorescence background, we functionalize a glass surface with BSA, neutravidin and superblock, with washing steps in between, as described before, and perform wide-field imaging (Fig. 1(f)). It is clear that the functionalization of the glass surface does not significantly contribute to the background signal.

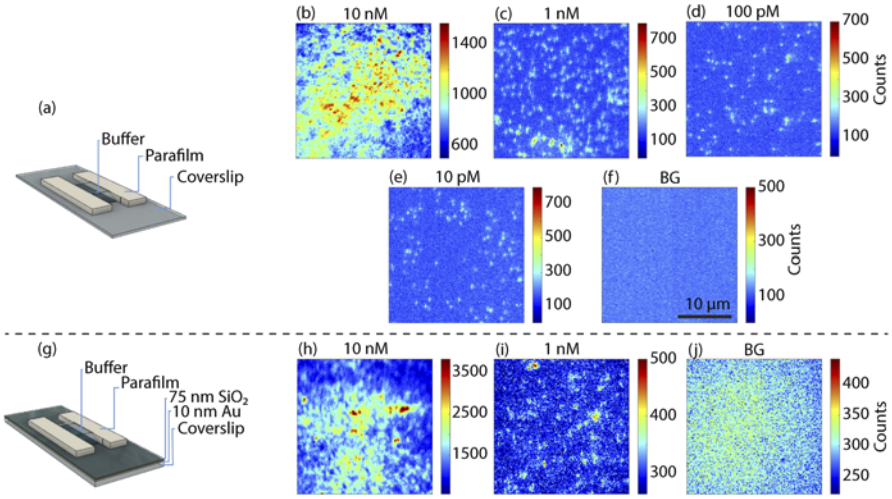

Fig. 1. Wide-field image of immobilized ATTO-647N labeled dsDNA. (a) Scheme of a glass coverslip flow channel. The channel is created between parafilm stripes to ease the washing process. (b-e) Data for samples prepared with different concentrations of ATTO-647N labeled dsDNA molecules (from 10 nM to 10 pM) in water on a glass coverslip flow channel. (f) Wide field image of T50, BSA, neutravidin and superblock (background) as a reference. The excitation power before the entrance of the microscope for (b-f) is 250 μW. (g) Scheme of a flow channel on the director substrate (director flow channel). (h-i) Wide field images of samples prepared with buffers at a DNA concentration of 10 nM and 1 nM on the director substrate. For samples prepared with concentrations below 1 nM, the molecules are hardly distinguishable from the background (not shown). (j) Background fluorescence image of the director substrate as a reference (before immobilization of ATTO-647N labeled dsDNA molecules). The excitation power before the entrance of the microscope for (h-j) is 827 μW. In all images the excitation wavelength is 636 nm and the integration time of the CMOS camera is 1 s. The scale bar for all figures is given in (f). The dark counts of the camera are around 100 and they are not subtracted.

The distribution of ATTO-647N labeled dsDNA molecules on coverslips and on a thin layer of SiO_2 is the same. Therefore, we expect to obtain the same molecular distribution on the director substrate as in the case of a glass coverslip flow channel. Figure 1(g) shows the scheme of a director flow channel and Fig. 1(h)-(i) represents the wide field image of samples prepared with DNA concentrations of 10 nM and 1 nM in water on the director flow channel. As shown in Fig. 1(j), the background of the gold substrate is high and 70% of the excitation light is reflected

Biomedical Optics EXPRESS

by the 10 nm gold layer. Therefore, it is difficult to observe the molecular distribution for samples prepared with DNA concentrations in water below 1 nM.

The collected fluorescence power (P_{fluo}) of an emitter in the planar antenna configuration is influenced by the fluorescence radiation pattern, the excitation power (P_{exc}) and the excited-state decay rate (Γ) [22]. Here, we simply probe these parameters for ATTO-647N in T50 by changing the reflector-director substrate distance. Since the back focal plane (BFP) imaging and decay rate measurements benefit from a higher number of detected photons, we choose samples prepared with DNA solutions at a concentration of 10 nM in water.

In Fig. 2(a) a scheme of the BFP imaging experimental setup is presented. The reflector is retracted step-wise from the relative zero position in the z-direction. Since ATTO-647N dye is prone to bleaching (see Fig. S2 of the Supplement 1), our approach is to decrease the measurement time as much as possible. This can be done either by step-size increasing or by decreasing the photon collection times. However, to construct BFP images using a CMOS camera, we cannot further decrease the acquisition time. Thus, a 20 nm step-size with an integration time of 2.2 s for each step seems like an appropriate solution.

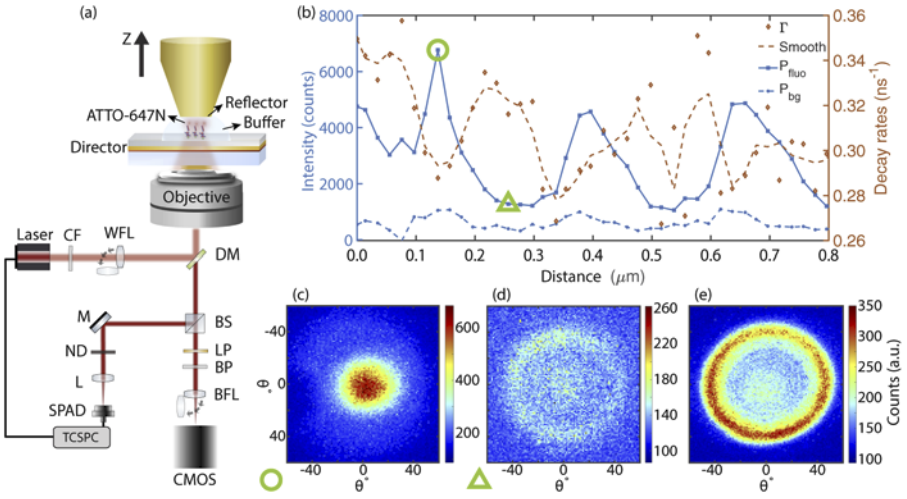

Fig. 2. ATTO-647N labeled dsDNA in the scanning planar antenna with liquid medium. (a) Schematic diagram of the scanning Yagi-Uda antenna configuration and the optical setup. The medium between reflector and director substrate is the T50 buffer. The sample was prepared from a solution of dsDNA molecules at a concentration of 10 nM in water. 95% of P_{tot} is detected by the CMOS camera and 5% is recorded by the SPAD. CF is a clean up filter, M is a mirror, L is a lens and WFL is a wide-field lens. (b) P_{fluo}, P_{bg} (counts) and the decay rate (ns^{-1}) as a function of distance between reflector and director substrate. The red dashed line is obtained by averaging three neighboring values of the decay rate. (c-d) The radiation pattern for two selected positions marked by a circle and a triangle in (b). (e) BFP image of ATTO-647N labeled dsDNA molecules immobilized in the coverslip flow channel.

The collected light from the sample is sent through the filter set and detected by the CMOS camera or the SPAD. The radiation pattern of the emitters is recorded by the CMOS camera. On the other hand, using TCSPC we construct a decay histogram. The integration of this histogram determines the total emitted power (P_{tot}), which comprises the fluorescence signal of the ATTO-647N dyes (P_{fluo}) and the background (P_{bg}). By deconvolving the decay histogram, using the instrument response function (IRF), one can plot the P_{fluo} and Γ as a function of distance between the director substrate and the reflector, as shown in Fig. 2(b). In this experiment the P_{bg}

Biomedical Optics EXPRESS

is much smaller than P_{fluo}, which gives us a SNR of 8.5 in the maximum of P_{fluo}. The peak to peak distance of P_{fluo} is 259 nm and it corresponds to $\lambda/2n$, where n is the refractive index of T50 (close to water) and λ is the emission wavelength of ATTO-647N (~680 nm).

Although P_{fluo} is not a smooth curve in Fig. 2(b), it is easy to observe that the intensity oscillates with the reflector-director substrate distance, as shown in Ref. [22], where the decay rate of fluorescence beads changes periodically in a scanning Yagi-Uda antenna. Here, however, the decay rate is not periodic after the first intensity peak, most likely due to scanning with larger steps and data points fitting (see Fig. S3 in the Supplement 1).

Additionally, in Fig. 2(c)-(d) we represent the BFP image of the emitted light at different selected distances marked by a circle and a triangle in Fig. 2(b). Figure 2(e) shows instead the emission pattern of ATTO-647N labeled dsDNA molecules on a glass coverslip (without a director nor reflector), which can be considered as the reference radiation pattern. Comparing Fig. 2(c) with Fig. 2(e), we notice that the radiation pattern changes from a ring shape to a "Gaussian-like" shape, with a full width at half maximum (FWHM) of 41° at the emission maximum. This beaming effect can have advantages in biosensing, because it can improve the collection efficiency and it allows us to reduce the numerical aperture of the optics (objective or fiber) without losing signal.

Figure 2 shows the fluorescence signal, the beaming effect and the modification of the decay rate for ATTO-647N dyes attached to dsDNA molecules, immobilized in the antenna at a concentration of 10 nM in water, with the space between reflector and director substrate filled with T50. For samples prepared starting from lower DNA concentrations in water, the number of molecules in the focal area is small. Thus the bleaching time of ATTO 647N plays an important role for longer measurements, and the bleaching of one ATTO-647N dye significantly changes the signal in a step-wise manner (see Fig. S2b-d of the Supplement 1).

For this reason, we modify the setup and manage to decrease the experiment time by a factor of 4. Moreover, to mitigate the bleaching process, our samples are excited using 2 μW laser power. The total fluorescence power P_{tot} is detected with SPAD1 and the laser reflection from the antenna P_{refl}, attenuated by a neutral density (ND) filter (OD=2), is recorded by SPAD2; a 95:5 beamsplitter is used to split the collected light into these two channels (Fig. 3(a)). Thus, we are able to determine the relationship between P_{refl} and the P_{tot} in order to compare the excitation power in different experiments.

Figure 3(b)-(c) plots P_{tot} and P_{refl} as a function of distance between reflector and director substrate. Since P_{tot} consists of P_{fluo} and P_{bg}, to subtract P_{bg}, we measure the sample in the scanning antenna configuration before (Fig. 3(b)) and after (Fig. 3(c)) the immobilization of ATTO-647N labeled dsDNA from buffered solution at a concentration of 1 nM.

In Fig. 3(b)-(c) the grey area shows the region, where the reflector and director substrate are in contact. The vertical dashed line goes through the maximum of the curve representing P_{tot} (blue curve) and the corresponding point of P_{refl} (red curve) determining the reflection value at a given distance.

In both Fig. 3(b) and Fig. 3(c) the oscillation amplitude of P_{refl} gradually decreases with distance between the reflector and director substrate. This phenomenon can be explained by the fact that, while the laser light remains focused on the director, the reflector is not able to refocus the incident laser light. P_{refl} exhibits the resonance of a cavity mode and the distance between two consecutive dips is $\lambda/2n$. Based on this relation and the fact that we can precisely control this distance using a piezo stage, it is possible to determine the refractive index n of the embedding medium. Here, n is 1.31, which is close to the refractive index of water (n_{water} = 1.33), as expected.

Moreover, since the antenna has a higher impact at sub-wavelength distances ($\lambda/6n$ to $\lambda/4n$), the first maximum of P_{tot} is 2.1 times higher than the second one (see Fig. 3(c)). On the other hand, the first reflection minimum is 1.5 times deeper than the second one.

Biomedical Optics EXPRESS

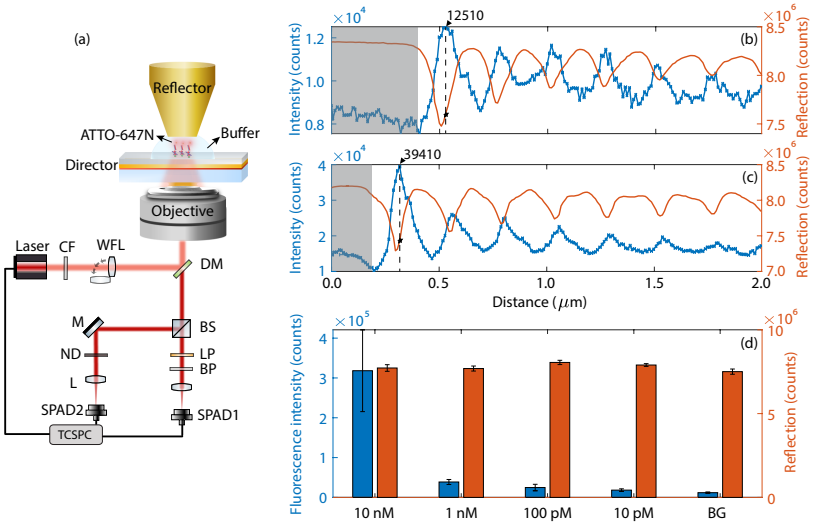

Fig. 3. Fluorescence intensity of ATTO-647N labeled dsDNA molecules immobilized in the planar antenna. (a) Scheme of the experiment. SPAD1 (SPAD2) detects P_{tot} (P_{refl}). (b,c) P_{tot} (blue curve) and P_{refl} (red curve) as a function of distance between reflector and director substrate (b) without ATTO-647N labeled dsDNA molecules and (c) with ATTO-647N labeled dsDNA molecules at a concentration of 1 nM. The maximum of P_{tot} in (b) is assumed as our background (BG). The grey region is the estimated area, in which the reflector and director substrate are in contact. This experiment takes around 55 s, (d) Average value of the maximum of P_{tot} and the corresponding P_{refl} for samples with different DNA concentrations. Each sample is measured with 2 μW excitation power.

We repeat this experiment for different spots of each sample prepared with buffers of various ATTO-647N labeled dsDNA concentrations (1 nM, 100 pM, 10 pM) and for the sample without such labeled dsDNA molecules. Figure 3(d) represents the averaged maximum of P_{tot} (blue bins) for samples with different molecule concentrations and the corresponding average of P_{refl} (red bins) at the position, where P_{tot} is maximal (see the cross section of the black dashed line and red curve in Fig. 3(b)-(c)).

In the samples, where the initial concentration of ATTO-647N labeled dsDNA molecules is very low (100 pM and 10 pM), the molecules attached to the surface are spatially well separated and the distance between them can be several micrometers in some cases. Therefore, if we choose measurement points randomly, most of the time we would collect only a background signal. To avoid this, at low concentrations we first try to find bright spots (fluorescent emitters) using wide-field imaging and only then we position the bright spots onto the focal point of the excitation beam. The downside of this approach is that most likely we select points with several emitters in the diffraction-limited spots, since they are more visible in wide-field imaging.

Therefore, we can associate the detected signal to a concentration with certainty, by our apparatus and sensing approach (i.e., by randomly choosing spots), only for samples prepared from solutions with a concentration of at least 1 nM, which corresponds to few (< 10) molecules in the detection spot. To better quantify the florescence signal, we would need to measure the mean concentration of molecules, for example, by knowing the illuminated area and the photon counts of a single molecule.

Figure 4(a) shows the same quantities of Fig. 3(d) for samples prepared with the coverslip flow channel. The significantly higher reflection signal in the antenna (Fig. 3(d)) compared to the coverslip is due to the high reflectivity ($\approx 70\%$) of the director. By subtracting the background

Biomedical Optics EXPRESS

from the fluorescence signal for each concentration in Fig. 3(d) and Fig. 4(a), one can calculate the fluorescence signal of the ATTO-647N dyes (P_{fluo}). In Fig. 4(b), P_{fluo} in the coverslip flow channel is compared with P_{fluo} in the antenna configuration for different ATTO-647N labeled dsDNA concentrations excited at 2 μW. We repeat the same experiment for the laser excitation power of 6.6 μW and the results are similar as in the case of 2 μW (not shown).

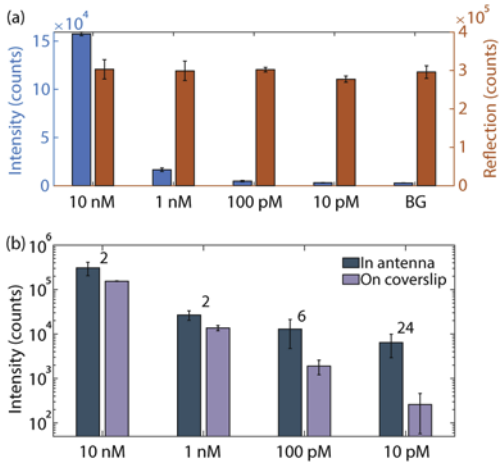

Fig. 4. Fluorescence of ATTO-647N labeled dsDNA molecules in the antenna and on the coverslip. (a) Average value of the maximum of P_{tot} and the corresponding P_{refl} for samples with different DNA concentrations on a glass coverslip. Each sample is measured with 2 μW excitation power. (b) Average background-corrected fluorescence signal of samples with different DNA concentrations on coverslip and in the antenna. The numbers above each bin represent the signal enhancement ratio.

Figure 4(b) determines that for samples prepared with higher DNA concentrations (10 nM and 1 nM) in antenna, the signal improves by a factor of 2, which is consistent with our previous work [22]. Here, such signal enhancement is caused mainly due to the modulation of the excitation rate. The beaming effect provides a minor change in the signal due collection with a high NA objective. If the NA becomes smaller, the beaming effect plays a significant role as the collection efficiency remains nearly the same for molecules in the planar antenna, whereas it drastically reduces for molecules on the coverslip. This increases further the antenna signal enhancement. On the other hand, since the results for samples prepared with DNA concentrations below 1 nM are obtained by pre-selection of the measurement points, it is difficult to compare them with the corresponding reference samples. To overcome this issue, a solution would be to perform a raster scan on the surface to increase the probability of excitation/detection of the fluorescent molecules.

4. Conclusion

In this work, we show that the fluorescence signal, the radiation pattern, and the decay rate of ATTO-647N dyes labeling dsDNA molecules immobilized in the antenna can be controlled by changing the distance between the reflector and director. Specifically, the radiation pattern changes from a doughnut-shape to a Gaussian-like profile (FWHM of 41°) and the fluorescence signal can be enhanced. This demonstrates the possibility of using low-NA optics, since by reducing the numerical aperture the collected fluorescence is not decreased. Therefore, this approach does not demand the use of microscopes [27] and it is also suitable for fiber-based detection [28,29].

Biomedical Optics EXPRESS

These findings motivate us to use this approach for biosensing in, e.g., in-vitro diagnostics. We show that ATTO-647N labeled dsDNA molecules in the antenna have at least a two-fold signal enhancement as compared to on a glass coverslip for the same analyte concentration in the buffer. Although one can detect single molecules with a planar antenna [21], our biosensor configuration is suitable for samples prepared from solutions with analyte concentrations down to 1 nM, which corresponds to few (below 10) molecules in the focal spot. For samples obtained from lower concentrations, one should use for instance raster scanning techniques in a small region (roughly 10 μm $\times$ 10 μm) of the sample, in order to obtain a signal proportional to the target molecule concentration. Finally, we argue that this technique can work for any fluorescence-based immobilized bioassay that fits in the space between reflector and director, while keeping the distance constraints.

Funding. Deutsche Forschungsgemeinschaft (INST 221/118-1FUGG, INST 221/131-1); Bundesministerium für Bildung und Forschung (13N14746); Universität Siegen.

Acknowledgments. The authors would like to thank A. Giannetti, P. Lombardi, C. Toninelli for helpful discussions and M. Hepp for experimental assistance. Part of this work was performed at the DFG-funded Micro-and Nanoanalytics Facility (MNaF) of the University of Siegen (INST 221/131-1) utilizing its major FIB/SEM instrument.

Disclosures. M. Agio et al. have filed the patent applications EP3283869, US2018128742 entitled "Device for the beaming of light emitted by light sources, in particular fluorescence of molecules" and EP16200599 entitled "Device for beaming and/or collecting of light emitted by a light source", which are related to this work.

Data Availability. Data underlying the results presented in this paper are not currently publicly available but may be obtained from the authors upon reasonable request.

Supplemental document. See Supplement 1 for supporting content.

References

1. A. J. Haes, L. Chang, W. L. Klein, and R. P. Van Duyne, "Detection of a biomarker for Alzheimer's disease from synthetic and clinical samples using a nanoscale optical biosensor," J. Am. Chem. Soc. **127**(7), 2264–2271 (2005).
2. Y. Lu, S. Peng, D. Luo, and A. Lal, "Low-concentration mechanical biosensor based on a photonic crystal nanowire array," Nat. Commun. **2**(1), 578 (2011).
3. S. M. Borisov and O. S. Wolfbeis, "Optical biosensors," Chem. Rev. **108**(2), 423–461 (2008).
4. I. Kucherenko, O. Soldatkin, D. Y. Kucherenko, O. Soldatkina, and S. Dzyadevych, "Advances in nanomaterial application in enzyme-based electrochemical biosensors: A review," Nanoscale Adv. **1**(12), 4560–4577 (2019).
5. E. Mauriz and L. M. Lechuga, "Plasmonic biosensors for single-molecule biomedical analysis," Biosensors **11**(4), 123 (2021).
6. S. Handschuh-Wang, T. Wang, S. I. Druzhinin, D. Wesner, X. Jiang, and H. Schönherr, "Detailed study of BSA adsorption on micro-and nanocrystalline diamond/β-sic composite gradient films by time-resolved fluorescence microscopy," Langmuir **33**(3), 802–813 (2017).
7. S. Firdous, S. Anwar, and R. Rafya, "Development of surface plasmon resonance (SPR) biosensors for use in the diagnostics of malignant and infectious diseases," Laser Phys. Lett. **15**(6), 065602 (2018).
8. P. Zijlstra, P. M. Paulo, and M. Orrit, "Optical detection of single non-absorbing molecules using the surface plasmon resonance of a gold nanorod," Nat. Nanotechnol. **7**(6), 379–382 (2012).
9. G. Qiu, Z. Gai, Y. Tao, J. Schmitt, G. A. Kullak-Ublick, and J. Wang, "Dual-functional plasmonic photothermal biosensors for highly accurate severe acute respiratory syndrome coronavirus 2 detection," ACS Nano **14**(5), 5268–5277 (2020).
10. S. Laing, L. E. Jamieson, K. Faulds, and D. Graham, "Surface-enhanced Raman spectroscopy for in vivo biosensing," Nat. Rev. Chem. **1**(8), 0060–19 (2017).
11. M. A. Ettabib, A. Marti, Z. Liu, B. M. Bowden, M. N. Zervas, P. N. Bartlett, and J. S. Wilkinson, "Waveguide enhanced Raman spectroscopy for biosensing: A review," ACS Sens. **6**(6), 2025–2045 (2021).
12. Y. Guo, H. Li, K. Reddy, H. S. Shelar, V. R. Nittoor, and X. Fan, "Optofluidic Fabry–Pérot cavity biosensor with integrated flow-through micro-/nanochannels," Appl. Phys. Lett. **98**(4), 041104 (2011).
13. A. Portela, O. Calvo-Lozano, M.-C. Estevez, A. M. Escuela, and L. M. Lechuga, "Optical nanogap antennas as plasmonic biosensors for the detection of miRNA biomarkers," J. Mater. Chem. B **8**(19), 4310–4317 (2020).
14. V. Flauraud, R. Regmi, P. M. Winkler, D. T. Alexander, H. Rigneault, N. F. van Hulst, M. F. García-Parajo, J. Wenger, and J. Brugger, "In-plane plasmonic antenna arrays with surface nanogaps for giant fluorescence enhancement," Nano Lett. **17**(3), 1703–1710 (2017).
15. J. Larkin, R. Y. Henley, V. Jadhav, J. Korlach, and M. Wanunu, "Length-independent DNA packing into nanopore zero-mode waveguides for low-input DNA sequencing," Nat. Nanotechnol. **12**(12), 1169–1175 (2017).
16. A. P. Demchenko, "Photobleaching of organic fluorophores: quantitative characterization, mechanisms, protection," Methods Appl. Fluoresc. **8**(2), 022001 (2020).

Biomedical Optics EXPRESS

17. S. Kühn, G. Mori, M. Agio, and V. Sandoghdar, "Modification of single molecule fluorescence close to a nanostructure: radiation pattern, spontaneous emission and quenching," Mol. Phys. **106**(7), 893–908 (2008).
18. A. G. Curto, G. Volpe, T. H. Taminiau, M. P. Kreuzer, R. Quidant, and N. F. van Hulst, "Unidirectional emission of a quantum dot coupled to a nanoantenna," Science **329**(5994), 930–933 (2010).
19. L. Novotny and N. Van Hulst, "Antennas for light," Nat. Photonics **5**(2), 83–90 (2011).
20. H. Aouani, O. Mahboub, N. Bonod, E. Devaux, E. Popov, H. Rigneault, T. W. Ebbesen, and J. Wenger, "Bright unidirectional fluorescence emission of molecules in a nanoaperture with plasmonic corrugations," Nano Lett. **11**(2), 637–644 (2011).
21. S. Checcucci, P. Lombardi, S. Rizvi, F. Sgrignuoli, N. Gruhler, F. B. Dieleman, F. S. Cataliotti, W. H. Pernice, M. Agio, and C. Toninelli, "Beaming light from a quantum emitter with a planar optical antenna," Light: Sci. Appl. **6**(4), e16245 (2017).
22. N. Soltani, E. Rabbany Esfahany, S. I Druzhinin, G. Schulte, J. Müller, B. Butz, H. Schönherr, N. Markešević, and M. Agio, "Scanning planar Yagi–Uda antenna for fluorescence detection," J. Opt. Soc. Am. B **38**(9), 2528–2535 (2021).
23. M. P. Busson, B. Rolly, B. Stout, N. Bonod, and S. Bidault, "Accelerated single photon emission from dye molecule-driven nanoantennas assembled on DNA," Nat. Commun. **3**(1), 962 (2012).
24. B. M. Reinhard, S. Sheikholeslami, A. Mastroianni, A. P. Alivisatos, and J. Liphardt, "Use of plasmon coupling to reveal the dynamics of DNA bending and cleavage by single EcoRV restriction enzymes," Proc. Natl. Acad. Sci. **104**(8), 2667–2672 (2007).
25. M. P. Busson, B. Rolly, B. Stout, N. Bonod, E. Larquet, A. Polman, and S. Bidault, "Optical and topological characterization of gold nanoparticle dimers linked by a single DNA double strand," Nano Lett. **11**(11), 5060–5065 (2011).
26. S. Ernst, D. M. Irber, A. M. Waeber, G. Braunbeck, and F. Reinhard, "A planar scanning probe microscope," ACS Photonics **6**(2), 327–331 (2019).
27. P. E. Lombardi, A. E. Giannetti, P. Cecchi, F. E. Chiavaioli, S. Howitz, N. Soltani, F. Sonntag, C. Toninelli, and M. Agio, "SEPSIS biomarker detection through lensless fiber-based planar antennas," Proc. SPIE **11772**, 117720N (2021).
28. N. Soltani and M. Agio, "Planar antenna designs for efficient coupling between a single emitter and an optical fiber," Opt. Express **27**(21), 30830–30841 (2019).
29. A. Giannetti, P. Cecchi, F. Chiavaioli, S. Howitz, P. Lombardi, N. Soltani, F. Sonntag, C. Toninelli, and M. Agio, "Sepsis biomarker detection through fiber-based planar antennas (conference presentation)," Proc. SPIE **11361**, 27 (2020).